Nitrogen-doped magnetic onion-like carbon as support for Pt particles in a hybrid cathode catalyst for fuel cells

Gang Wu,†* Changsong Dai, Dianlong Wang, Deyu Li and Ning Li

Received 16th November 2009, Accepted 16th January 2010
First published as an Advance Article on the web 22nd February 2010
DOI: 10.1039/b924010a

Pt and non-precious metal catalysts were combined to build a hybrid cathode for fuel cell application, with the aim of dramatically reducing the amount of Pt and increasing the overall catalytic performance. An active nitrogen-doped magnetic onion-like graphitic carbon material (N-Me-C) was synthesized by pyrolyzing a hexamethylene diamine-Me (Me: Co and Fe) complex. The N-Me-C materials proved capable of effectively catalyzing the oxygen reduction reaction (ORR), as evidenced by rotating disk/ring electrode (RDE/RRDE) data showing significant positive shifts of onset and half-wave ($E_{½}$) potentials and a drop of H_2O_2 yield, when compared to traditional carbon supporting materials. In the hybrid cathode catalyst, ultra-low loading Pt nanoparticles (2 wt%) were subsequently anchored to the N-Me-C support through a chemical reduction method. The configuration using ultra-low Pt loading is advantageous for mitigating particle agglomeration and improving Pt utilization due to isolated particle distributions and smaller particle sizes. Electrochemical and fuel cell data confirmed that the use of the N-Me-C support leads to a significant enhancement of ORR catalytic activity. It is quite significant that the 2% Pt/N-Me-C cathode with an ultra-low Pt loading of 0.04 mg_{-Pt} cm^{-2} is effective in generating a current density of *ca.* 0.14 and 0.59 A cm^{-2} at cell voltages of 0.80 and 0.65 V operated in a H_2-air cell, respectively. The corresponding mass activity (A mg_{-Pt}^{-1}) was increased by factors of 1.4 and 3.5 at 0.65 V, when compared with 2% Pt/C and commercial E-TEK 20% Pt/C cathodes. Extensive physical and electrochemical characterization revealed that the significant improvement in mass activity is mainly attributable to the non-precious ORR active sites on M-Me-C, and also partially to the beneficial support effect of nitrogen doping associated with stronger support-metal interactions and smaller particle sizes.

Introduction

Polymer electrolyte fuel cells (PEFCs) have long been actively recognized as potential automotive and stationary power sources owing to their rather high efficiency, and low environmental impact. However, their ultimate commercialization continues to be hindered due to the current use of expensive and limited-supply Pt catalysts resulting in prohibitive costs. While the precious metal is used for both PEFC electrodes, much larger quantities of Pt are required for the cathode because of the significantly lower rate of oxygen reduction kinetics than that of hydrogen oxidation in the fuel cell anode.[1,2] It is generally believed that the large-scale application of fuel cells will be difficult to realize if the expensive Pt for the oxygen reduction reaction (ORR) cannot be mostly replaced by other efficient, low-cost, and stable electrodes.[3] To overcome this barrier, much effort has been made in developing an effective Pt-based alloy with higher precious metal utilization,[4] and even alternative non-precious metal catalysts.[5,6] In exploring the non-precious metal catalysts, although substantial progress has been achieved in the synthesis, performance improvement, and understanding of the ORR mechanism, practical resolution regarding its long-term durability and high activity in fuel cells is still far from effective.[7–9] In addition, a much thicker non-precious catalyst layer (*ca.* 100 μm) badly restrains mass transfer (H^+, O_2 and H_2O) and causes severe flooding in the cathode, a major issue with PEFCs.[8,10]

To this end, we are conceiving a novel strategy to develop a hybrid cathode catalyst consisting of precious Pt (with low loading) and non-precious catalysts (as supporting materials), thereby maintaining a reasonable balance between costs and ORR performance. In doing so, well-dispersed Pt nanoparticles would be supported on active carbon-based non-precious catalysts. Thus, a primary challenge for this conception is to develop a non-precious carbon material capable of high ORR activity and stability. Among many attempted formulations, catalysts obtained by simultaneously heat-treating precursors of transition metals and nitrogen have shown the most promising activity in acid media, leading to a new group of non-precious cathode catalysts as an alternative to Pt.[11] To date, even though the nature of ORR active sites on such-fabricated catalysts has not been unambiguously determined, effective carbonization of organic compounds in the presence of transition metal species to form nitrogen-doped graphitic carbon has been commonly accepted as chemical and morphological necessities for inducing efficient multi-electron transfer ORR catalysis. There is little doubt that nitrogen functionalities (pyridinic or quaternary nitrogen) are tied to ORR activity on the carbon surface.[7,12–14]

Department of Applied Chemistry, Harbin Institute of Technology, Harbin 150001, China
† Present address: Los Alamos National Laboratory, MPA-11, Los Alamos, New Mexico 87545, USA. E-mail: wugang@lanl.gov; Fax: +1-505-665-4292; Tel: +1-505-667-3060

So, nitrogen-doped carbon seems to be the most suitable ORR active material to support Pt particles in the hybrid cathode catalyst.

Aside from being an active catalyst itself, the nitrogen-doped carbon material possesses many advantageous support effects over a non-doped one in metal catalysts.[15–19] There has been increasing evidence showing that a nitrogen dopant has profound impact on surface states, electron-transfer rates, and adsorption for electrocatalysis processes. As surface chemistry and morphology of the support materials can greatly influence catalytic activity and stability through enhancing the support-metal interactions, and consequently modifying the electric structure of catalytic metals,[20–26] the nitrogen-doped carbon supports would offer a new opportunity to tailor chemical/physical properties of loaded metal particles.[27] Our previous work indicated[18,19] that the use of a nitrogen-doped carbon support leads to enhanced mass activity (Pt utilization) and intrinsic activity (charge-transfer rate) in methanol oxidation on Pt and PtRu catalysts. On nitrogen-doped carbon supports, the dislocations, curvature and other defects arising from the doping of nitrogen atoms could serve as active sites to anchor reduced Pt seeds. In addition, doping of nitrogen atoms into carbon not only geometrically modifies surface structures, but also influences the surface pK_a values. On non-doped carbon materials, pH_{pzc} values are typically near or below 7.0, dictated by acidic oxygen-containing functionalities. It was reported[28] that nitrogen-doped carbon nanotubes (N-CNTs) with 4.0 atom% nitrogen possess a much more alkaline pH_{pzc} value of 9.3 due to the prevalence of negatively charged nitrogen functionalities showing more reductive character. Using iodimetric analysis, a correlation between nitrogen content and the number of reducing sites is apparent, with triple the number of active sites observed for N-CNTs containing 7.5 at% nitrogen over non-doped CNTs.[28] Theoretically, the pyridinic and quaternary nitrogen atoms link to two and three sp^2 carbon atoms and contribute one and two P_π electrons in the graphitic π system, respectively.[29] As a consequence, the richness in local electron density and surface energy differences might facilitate the nucleation and growth of metal particles on the N-doped supports, resulting in a stronger metal-support interaction.[19,27] More importantly, in oxygen reduction, the nitrogen-induced charge delocalization could also change the chemisorption mode of O_2 from the usual end-on adsorption (Pauling model) on carbon to a side-on adsorption (Yeager model) onto the N-doped carbon electrodes.[5] The parallel diatomic adsorption could effectively weaken the O-O bonding to facilitate oxygen reduction.

In an effort to synthesize this kind of nitrogen-doped carbon material, the use of a wide variety of nitrogen-containing chemicals (NH_3, acetonitrile, amine, polyaniline, polypyrrole, *etc.*) and transition metals (Fe, Co, Ni, Cu, Mn, V, Cr, *etc.*) has been attempted. However, ORR catalytic activity on such fabricated nitrogen-doped carbon was found to be strongly dependent on the nitrogen precursor, transition metal, and synthesis strategy.[8,30,31] Experiments indicated that iron and cobalt are more efficient than other metals in inducing nitrogen atom doping into carbon structures and larger molecule nitrogen compound-derived catalysts seem to generate higher activity than smaller ones.[7,8] Hexamethylene diamine (HDA), a kind of diamine consisting of a hexamethylene hydrocarbon chain, was newly employed as nitrogen precursor to chelate with transition metals (Co and Fe), and synthesize nitrogen-doped carbon materials in this work. It is of note that a novel onion-like graphitic carbon nanostructure was formed during the pyrolysis step in the synthesis. Onion-like graphite structures have been considered as quasi-spherical nanoparticles consisting of fullerene-like carbon layers enclosed by concentric graphitic shells, but their electronic structures of π and σ is different from those of graphene.[32] Apart from potential advantages in electrocatalysis due to its highly symmetric structure and hybrid orbital (sp^2, sp^3, and $sp^{2.278}$), onion-like carbon possesses a high degree of graphitization structure, which would be a beneficial feature as supporting materials in electrocatalysis,[33] ensuring higher electron conductivity, a stronger support-metal interaction, and a better corrosion resistance. Thus, it is of importance to utilize the remarkable support effect in a Pt catalyst to catalyze oxygen reduction. As a consequence, the synthesized carbon composite materials, featuring doping of nitrogen, and unique onion-like nanostructure were used to support Pt nanoparticles with a loading around 2.0 wt%. The usage of the ultra low-loading of Pt catalyst is advantageous for mitigating agglomeration of Pt particles and improving Pt utilization due to the relatively long distances among particles and small particle sizes, as Pt particles tend to grow larger and agglomerate together with an increase in loading.[19,34–36] Informative insights into the origin of the ORR performance enhancement by using the newly developed carbon composite support also were discussed based on extensive physical and electrochemical characterization.

Experimental

Materials synthesis

Carbon support, a commercial Ketjenblack EC 300J, with a Brunauer-Emmett-Teller (B.E.T.) surface area of about 950 m^2 g^{-1} and good corrosion resistance,[37] was treated in 1.0 M HCl solution for 24 h at room temperature to remove any potential metal impurities. HDA ($H_2N(CH_2)_6NH_2$), a kind of diamine, was employed to chelate with transition metals (Fe and Co). In a typical approach, transition metal salts, 0.01 mol $FeCl_3$ and 0.01 mol $Co(NO_3)_2 \cdot 6H_2O$ (Fe : Co = 1 : 1 atom ratio) were first added into 0.5 M HDA ethanol solution, then kept rigorous stirring for 4 h. It is worth noting that, when transition metals were mixed with HDA, a dark-yellow suspension gradually appears, suggesting the formation of an interlinked HDA-Me complex. Subsequently, 0.40 g pre-treated carbon support was mixed with the above complex. After constant stirring for 12 h to allow the complex to fully impregnate into carbon, the suspension was vacuum-dried using a rotary evaporator and then heat treated at 900 °C in flowing nitrogen gas for one hour. The resultant pyrolyzed sample with a typical amount of 0.30 g was leached in 300 ml 0.5 M H_2SO_4 at 80 °C for 8 h to remove unstable and inactive species from the catalyst, and then thoroughly washed in de-ionized water.[8,38] The purpose of the pre-leach in an acid solution is to maintain a stable catalyst in an acidic Nafion®-based fuel cell. Finally, the product was denoted here as N-Me-C. In order to explore the roles of nitrogen and transition metals in ORR catalysis, a nitrogen-doped carbon sample (denoted as N-C) was prepared identically except for the

omission of transition metals from the recipe. A carbon black sample (denoted as C) treated with pyrolysis and acid leach steps omitting nitrogen precursor and transition metals also was used as a comparison.

The carbon supported Pt catalysts were prepared through the so-called formic acid method (FAM).[19] Briefly, an appropriate mass of N-Me-C was ultrasonically suspended in $H_2PtCl_6 \cdot 6H_2O$ + HCl solution containing a given Pt amount to maintain a nominal Pt loading of 2.0 wt% *versus* supporting materials. The configuration with a low Pt loading is advantageous for improving Pt utilization and mitigating particle agglomeration due to small particle sizes and isolated particle distributions. When the mixture was heated to 80 °C, 100 ml formic acid solution (30%) was slowly added in drops. Under a rigorous magnetic stir at 80 °C for 24 h, the suspension was left to cool at room temperature; and the solid was filtered and dried in a vacuum oven at 80 °C overnight. Consequently, N-Me-C supported Pt catalyst with a desirable Pt loading was obtained and denoted as 2% Pt/N-Me-C. For the sake of comparison, Pt nanoparticles also were deposited on pyrolyzed and acid-treated carbon black support under an identical procedure, denoted as 2% Pt/C catalyst.

Physical characterization

These samples were characterized by X-ray photoelectron spectroscopy (XPS) using an ESCA 210 and MICROLAB 310D spectrometer for elemental quantification and specie analysis. For recording the spectra, Mg-Kα irradiation was employed as X-ray source. High resolution spectra were acquired at 20 eV pass energy. Area of analysis is 700 × 300 microns in size, and each sample was analyzed for 90 degrees take-off angle (TOA) with a depth of 8–10 nm. The crystallinity of the samples was determined by X-ray diffraction (XRD) performed on an automated Rigaku diffractometer equipped with a Cu-Kα radiation and a graphite monochromatic operation at 45 kV and 40 mA. The diffraction patterns were scanned at a rate of 1.2 deg min^{-1} with a step of 0.02 deg. High-resolution transmission electron microscopy (HR-TEM) images were taken on a JEOL JEM-2010F microscope with a resolution of 0.102 nm operating at 200 kV.

RDE and RRDE measurements

ORR activity and four-electron selectivity were electrochemically evaluated using RDE/RRDE electrodes. All measurements were performed using a CHI electrochemical station (Model 750b) in a conventional three-electrode cell with 0.5 M H_2SO_4 electrolyte at room temperature. Graphite rod and standard $Hg/HgSO_4$ were used as the counter and reference electrodes, respectively. All potentials in this work have been converted to the normal hydrogen electrode (NHE) scale. To deposit the catalyst onto the disk electrodes, a 10.0 mg catalyst sample was ultrasonically dispersed in 1.0 ml isopropanol for 30 min to form a "catalyst ink". Then, a given amount of the ink and 5 μl 5% Nafion® solution were applied to the glassy-carbon disk. In RDE tests, ORR steady-state polarization curves were recorded in O_2 saturated 0.5 M H_2SO_4 solution with a potential step of 0.03 V and a period time of 30 s from 0.1 to 1.0 V with positive-going at a rotating rate of 900 rpm. Prior to the RRDE experiment, the Pt ring was activated by potential cycling in N_2-saturated 0.5 M H_2SO_4 solution from 0 to 1.4 V at a scan rate of 50 mV s^{-1} for 10 min. The ring potential was set to 1.2 V to oxidize the H_2O_2, a deleterious intermediate only transferring two electrons in ORR. So four-electron selectivity of catalysts can be evaluated based on measured H_2O_2 yield.[39] Cyclic voltammetry (CV) of Pt samples was typically recorded in the potential range from 0 to 1.0 V at a scan rate of 10 mV s^{-1} in N_2-saturated 0.5 M H_2SO_4 electrolyte.

Fuel cell testing

These synthesized Pt catalysts were tested as fuel cell cathodes to evaluate their ORR activity under PEFC operating conditions. Catalyst ink was prepared by ultrasonically mixing catalyst powders with a Nafion® solution for four hours and applied to the gas diffusion layer (GDL, ELAT LT 1400W, E-TEK) by successive brushing until the total cathode catalyst loading of 2 mg cm^{-2} (0.04 $mg\text{-}_{Pt}$ cm^{-2}) was reached. The Nafion® content in the dry catalyst was maintained at around 35 wt%. A commercially available Pt-catalyzed gas-diffusion electrode, (E-TEK, 0.25 mg cm^{-2} Pt) was used at the anode. The cathode and anode electrodes were hot-pressed onto a Nafion® 212 membrane with a geometric area of 5.0 cm^2. Fuel cell testing was carried out in a single cell with serpentine flow channels. Pure hydrogen and air humidified at 85 °C were supplied at a flow rate of 200 and 400 mL min^{-1}, respectively. The cell temperature was set to 80 °C and back pressure for both anode and cathode was maintained at 30 psig. Fuel cell polarization plots were recorded using standard fuel cell test stations.

Results and discussion

Magnetic property of N-Me-C

The magnetic property of the carbon composite support (N-Me-C) was qualitatively demonstrated using photographs of

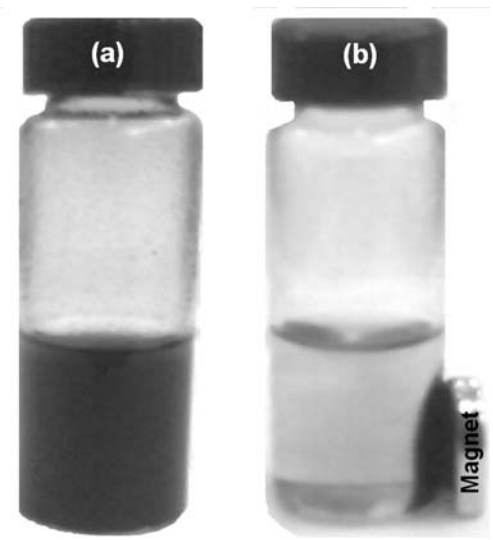

Fig. 1 Photographs of N-Me-C dispersion in an aqueous solution (a) before and (b) after magnetic separation.

N-Me-C dispersion in an aqueous solution before (Fig. 1a) and after (Fig. 1b) magnetic separation by applying an external magnet. This suggested that the metallic aggregates were produced during the pyrolysis step. While the server acid leaching step is able to mostly resolve these Co/Fe species, those encapsulated into a carbon structure probably can survive, showing a magnetic feature. To date, the promotional roles derived from transition metals in an enhancement of ORR activity for such-fabricated carbon composite have not been unambiguously determined, remaining the subject of much debate. While Dodelet *et al.*[11,14] provided data indicating that the ORR active site involves MeN_x/C-type species (Me: Co and Fe), other researchers[13,28,40,41] suggested that, rather than participating directly in active sites for ORR, transition metals just play roles in the formation of active sites by catalyzing doping of nitrogen atoms into carbon or electronically changing their environment.

XPS analysis

XPS was employed to study the composite carbon supports and loaded Pt particles. The survey spectra for N-Me-C, 2% Pt/N-Me-C and 2% Pt/C are compared in Fig. 2a and their elemental quantification is summarized in Table 1. C, O and N elements were detected, but no Co/Fe species were observed with the N-Me-C sample. This indicated that the metal species on the catalyst surface are chemically resolved in acid solution, whereas the metallic species encapsulated into a carbon structure could survive, evidenced by the magnet demonstration in Fig. 1. An obvious Pt signal for 2% Pt/N-Me-C and 2% Pt/C samples confirmed that Pt particles were anchored on both N-Me-C and traditional carbon black supports. Actual Pt loadings for these two catalysts are around 1.8 and 1.9 wt%, respectively, which are very close to the nominal value 2 wt%. The slightly reduced Pt content is probably due to additional introductions of doped nitrogen atoms and oxygen-containing functional groups. We therefore still use the nominal value (2 wt%) to label these Pt catalysts. Importantly, the presence of nitrogen species on 2% Pt/N-Me-C sample suggests that nitrogen functional structures remain on the carbon support after depositing Pt particles. Fig. 2b shows a comparison of high-resolution N 1s spectra between nitrogen-involving N-C and N-Me-C samples to elaborate the effect of metals on nitrogen doping into carbon structures. It was believed that the nitrogen atoms could incorporate into the graphene layers to replace carbon atoms at different sites during the pyrolysis process (above 700 °C), thereby showing various binding energies in the XPS spectra.[29] Among them, the nitrogen atoms doped at the edges of the graphitic carbon layers with a binding energy of 398.6 ± 0.3 eV are referred to as pyridinic N (N-6) and the quaternary nitrogen (N-Q) is defined as a nitrogen atom that dopes inside the graphitic carbon layer with a relatively higher binding energy (401.3 ± 0.3 eV).[13,42] Therefore, two dominant peaks around 398.6 and 401.3 eV observed with these N-C and N-Me-C samples can be attributed to pyridinic and quaternary nitrogens, respectively. This suggests that the nitrogen atoms, regardless of the presence of transition metals, are able to dope into the carbon structures, replacing the carbon atoms both at the edges and inside of the graphitic carbon structures. However, when compared with the N-C sample, the N-Me-C sample exhibits a relatively higher intensity for

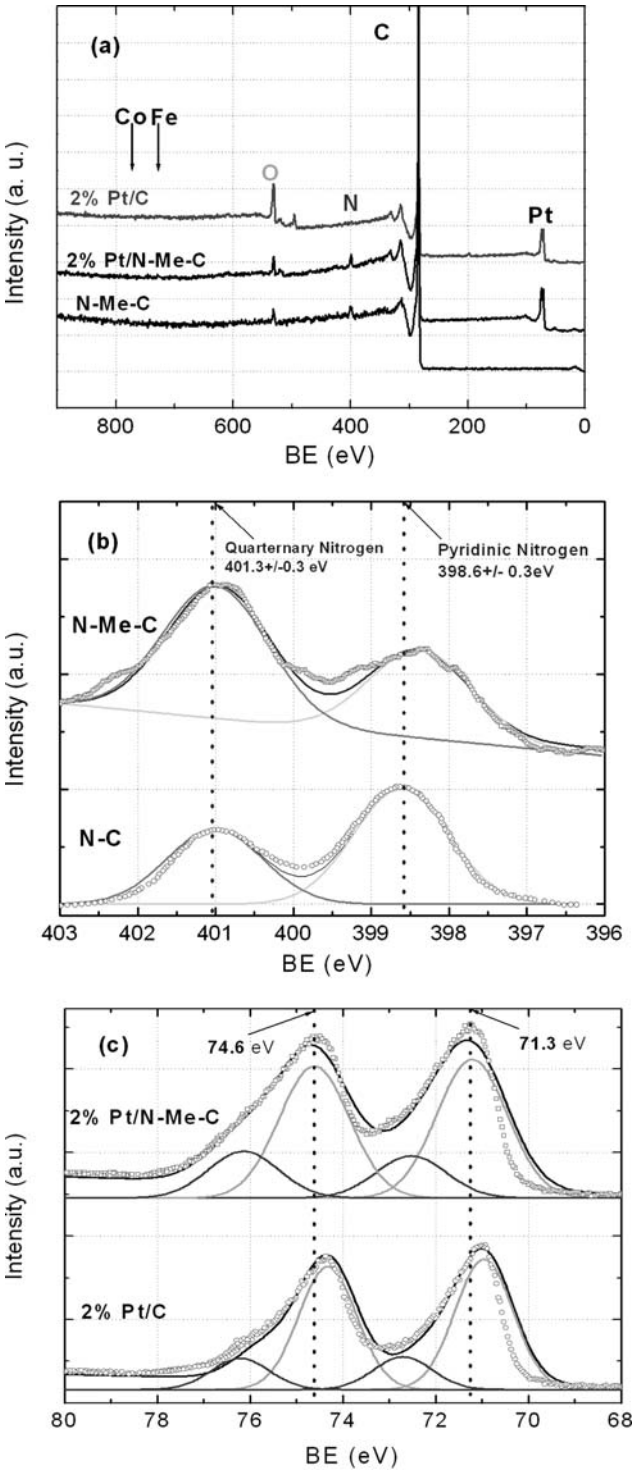

Fig. 2 (a) XPS survey spectra for various samples, (b) N 1s, and (c) Pt 4f.

quaternary nitrogen peak, revealing that, in the presence of transition metals, doping of nitrogen atoms favors the replacement of carbon atoms at the interior, rather than at the edges of the graphene layer. It has been reported[13,18] that during the pyrolysis of carbon containing nitrogen groups, pyridinic nitrogen can be gradually converted to quaternary one until equilibrium is achieved. It can, therefore, be presumed that addition of transition metals shifts the equilibrium of nitrogen

Table 1 Elemental quantification for various catalysts by XPS high-resolution survey

	Elemental quantification (wt%)					
Catalyst	C	N	O	Co	Fe	Pt
N-Me-C	92.4	4.5	3.1	0	0	0
2% Pt/N-Me-C	90.1	4.1	4.0	0	0	1.8
2% Pt/C	91.2	0	6.9	0	0	1.9

doping towards the higher quaternary nitrogen direction by accelerating this conversion. The XPS analysis was also used to compare the metal-support interactions in Pt catalysts as shown in Fig. 2c. The most intense doublet peaks (near 70.8 and 74.2 eV) assigned to Pt(0) in the 2% Pt/C catalyst were found to positively shift to higher binding energies (71.3 and 74.6 eV) in the 2% Pt/N-Me-C, possibly due to a stronger interaction between Pt particle and N-doped carbon support, resulting from the richness in local electron density to facilitate the deposition of reduced Pt seeds on the support. Such shifts in binding energy also had been reported in CNTs-supported Pt catalysts, showing enhanced electrocatalytic activity for methanol oxidation.[24,25]

XRD analysis

XRD patterns for various carbon samples (C, N-C, N-Me-C) and Pt catalysts (2% Pt/N-Me-C and commercially available E-TEK 20% Pt/C) are shown in Fig. 3. In these carbon samples, the strongest peak around $2\theta = 24.5–25.5°$ corresponds to the (002) basal plane diffraction in the graphitic structure. The broad (002) peaks can be attributed to two separate forms of carbon cited as turbostratic carbon (amorphous carbon) and graphene carbon (graphitic carbon).[43] It is worth noting that the nitrogen-doped carbon samples (N-C and N-Me-C) display a slightly positive shift in the C (002) peak when compared with the non-doped carbon black sample. This is partially attributed to a better graphitic crystalline structure possibly related to nitrogen doping. The improved graphitic character has been confirmed in

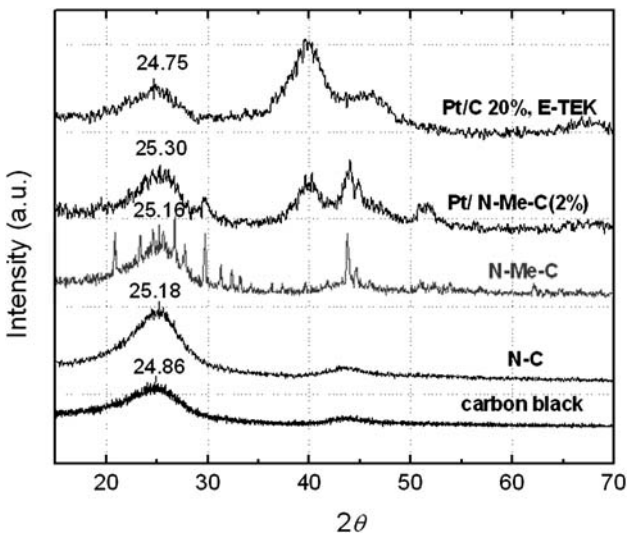

Fig. 3 XRD patterns for both non-Pt and Pt samples.

CN_x films using electron spin resonance (ESR) and Raman analyses.[44] In addition, the positive shift of (002) peak in XRD pattern probably is due to a decrease of *d*-space of (002) crystal plane arising from nitrogen doping, leading to more compact graphitic structures in comparison to those of pristine carbon black.[44,45] In the case of N-Me-C, metallic Co (JCDPS 15-0806), Fe (JCPDS 06-0696), FeO (JCPDS 06-0615), Fe_2O_3 (JCPDS 87-1166) and Fe_3O_4 (JCPDS 19-0629) aggregates[46] were detected. The metallic Co/Fe aggregates proved to be formed in pyrolysis. However, during acidic treatment, while the metal species on the surface would be leached out, that which is encapsulated can remain under the carbon structure. This is the reason why XPS is unable to collect the dominant signal from the metal species, but XRD and magnetic separation experiments obviously suggest their existence in the N-Me-C sample. The peaks assigned to metallic Co and Fe phases also were detected in the pattern of 2% Pt/N-Me-C at $2\theta = 29.6°$, 33.7°, 44.8°, 43.9°, 51.1°, 51.8°, 65.5° and 75.0°. Being consistent with commercial E-TEK 20% Pt/C catalyst, the peaks at the 2θ value of 39.7°, 46.2°, and 67.5° in 2% Pt/N-Me-C sample are characteristic diffraction peaks for Pt (111), (200), and (220) planes (JCPDS 04-0802), respectively,[47,48] but showing relatively low intensity due to the significantly low Pt loading. Like the N-Me-C sample, a slightly higher 2θ value of C(002) in the 2%Pt/N-Me-C sample also was observed due to the nitrogen doping as discussed.

HR-TEM analysis

The representative HR-TEM images for nitrogen-doped onion-like magnetic carbon at various magnifications and local areas are shown in Fig. 4. It can be clearly seen that the onion-like graphitic carbon nanostructures were formed in the N-Me-C sample during the pyrolysis of the cross-linked HDA-CoFe complexes. Noteworthy, both metal-encapsulated (Fig. 4c and 4d) and hollow (Fig. 4e and 4f) onion-like nanostructures represented by concentric spherical graphitic shells can be clearly observed. These metallic particles were identified as Co and Fe species using energy dispersive spectroscopy (EDS) coupled with HR-TEM, as shown in the insert of Fig. 4b. The hollow carbon nanostructure probably is due to the result of the dissolution of metal particles from the graphitic carbon shells during the acidic treatment with 0.5 M H_2SO_4 acid. The outer diameter size of the spherical graphitic shell structures is between 2 and 5 nm. The distance between the two graphitic planes in the onion-like shells was determined to be 0.28 nm (Fig. 4f). This value is slightly shorter than that of the interplanar distance in a pristine graphite structure (0.34 nm),[49] probably due to the nitrogen atoms doping into graphite planes as discussed in XPS and XRD analyses. Incomplete spheroidal shells (Fig. 4e) also could be found in these HR-TEM images, indicating that the onion-like structure obtained from pyrolysis in this work is not as well ordered as ones synthesized by annealing nano-diamond.[50–52] The possible growth mechanism for the metal-encapsulating online-like carbon in this work can be approximately proposed based on a vapor-liquid-solid model[53] as shown in Fig. 5. Briefly, during thermal treatment in an inert atmosphere at 900 °C, HDA-CoFe complexes were decomposed into gaseous carbon, nitrogen and metal species simultaneously. Metal atoms were first congregated into active metallic nanoparticles, then gaseous carbon and

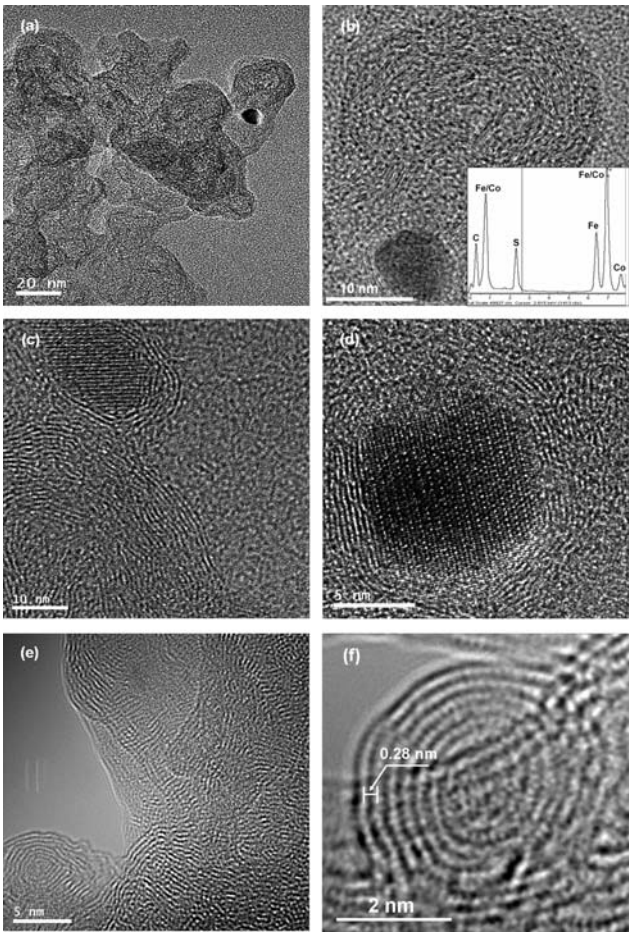

Fig. 4 Representative high-resolution TEM images for nitrogen-doped magnetic onion-like carbon supporting materials at various magnifications and areas: (a) overall morphology, (b) magnified incorporated metal aggregate, (c) and (d) metal-encapsulated onion-like carbon, and (e) and (f) hollow onion-like carbon nanostructures.

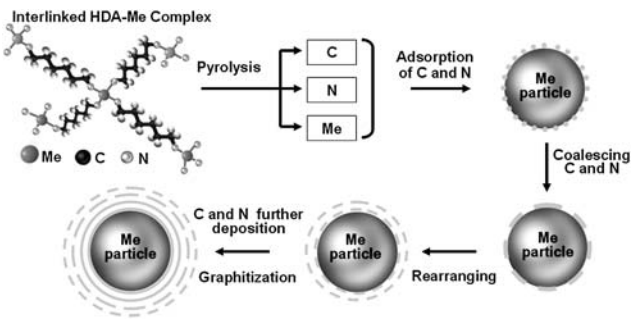

Fig. 5 Growth model of magnetic N-Me-C onion-like graphitic carbon.

nitrogen species were gradually captured by these metal nanoparticles, and immediately further decomposed into carbon and nitrogen atoms due to the catalytic functions of Co and Fe metals. Meanwhile, these atoms were precipitated and cooled down to form small nitrogen-doped carbon fragments around these encapsulated metal particles. The structural defects, especially the dangling bonds at the edges of these fragments, possibly act as nucleus for further assembly and rearrangement, finally forming a layered structure on the surface of metal particles. It is worth noting that small graphitic layers coalesced from the dangling bonds at the edges of carbon fragments are not definitely concentric to each other, thereby usually forming discontinuous graphitic layers such as dislocations and irregular curvature. Moreover, the intrusion of nitrogen atoms suppresses surface diffusion of carbon atoms during graphitization, leading to more disorder and compact structures in these graphite sheets.[44] Apart from other potential advantages, the electron conductivity in electrocatalysis would benefit from the layered onion-like graphitic carbon nanostructures due to the high crystallinity as illustrated by these HR-TEM images. Also, the highly graphitizing onion-like carbon nanostructure is favorable to improve its corrosion resistance and catalyst stability,[54] as carbon materials tend to be oxidized to CO and CO_2 under PEFC operating conditions, leading to a catalyst degradation.[23] The use of onion-like graphitic carbon, therefore, would be capable of improving the catalyst durability.

The HR-TEM image in Fig. 6a illustrates the isolated and scattered particle morphology for the 2 wt% Pt/N-Me-C catalyst, due to its ultra-low loading. The mean particle size determined from the image is around 2.0 nm. At the same time, the image for the 2% Pt/N-Me-C catalyst subjected to 5000 cycles between 0 and 1.0 V in N_2-saturated 0.5 M H_2SO_4 was compared in Fig. 6b. It can be seen that the size of the Pt particle and distribution are nearly identical around 2–3 nm (the inset of Fig. 6b) after such long-term electrochemical cycling. In the case of commercial E-TEK 20% Pt/C catalyst, it had been reported that, after similar cycling test in RDE, the average particle size is increased from *ca.* 3 nm to *ca.* 7 nm, and some aggregated Pt nanoparticles are as large as 15 nm.[26] During PEFC operation, Pt nanoparticles usually agglomerate or fall off from the carbon support, resulting in the decrease in the electrochemically active surface (EAS) area and consequently performance degradation.[35] Here, ultra low-loading morphology would decrease the coarsening and agglomerate probability of Pt particles due to their isolated and scattered particle distribution. More importantly, the enhanced interaction between Pt particles and N-doped carbon supports could make particles more strongly anchored onto carbon, and mitigate their accumulation. This point could be further supported by relevant evidences from the recent model catalytic systems proposed by O'Hayre and his co-workers.[27] Surface energy measurements, estimated from water-droplet contact angle, indicated that doping of nitrogen could change a hydrophobic state for the highly oriented pyrolytic graphite (HOPG) to a more hydrophilic condition. This change qualitatively reveals nitrogen doping leads to a higher energy

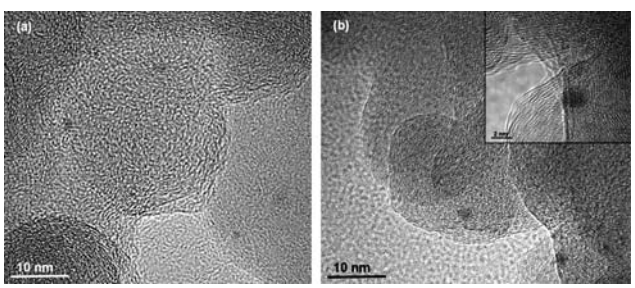

Fig. 6 High-resolution TEM images for 2% Pt/N-Me-C catalyst before (a) and after (b) 5000 cycles in N_2-saturated 0.5 M H_2SO_4 electrolyte.

surface, presumably due to the increased roughness, structural disorder, creation of dangling bonds, and introduction of polar functionalities.[27] As a consequence, Pt migration and coarsening on N-doped HOPG substrates have been significantly impeded due to these modifications in both physical geometric defects and chemical doping.

CV characterization

Compared with N-Me-C supporting materials, well-defined hydrogen absorption-desorption features are clearly seen in CV curve for the 2% Pt/N-Me-C in N_2-saturated 0.5 M H_2SO_4 solution at room temperature, as shown in Fig. 7. EAS of platinum can be estimated from the integrated charge in the hydrogen desorption peak (absorption peak was merged in capacitive background). After normalizing to the mass of Pt in the catalyst, EAS can be calculated from eqn (1)

$$EAS = \frac{Q_H}{M_{Pt} Q_{Href}} \quad (1)$$

where Q_H is the amount of charge for the electro-desorption of hydrogen atoms on the Pt surface, and M_{Pt} is the mass of Pt. Q_{Href} is assumed to be 0.21 mC cm^{-2} corresponding to a surface density of 1.3×10^{15} atom cm^{-2} of Pt.[55] Thus, the calculated value of EAS for 2% Pt/N-Me-C is around 130 m^2 g^{-1}, which is much higher than that of conventional E-TEK 20% Pt/C catalyst (*ca.* 80 m^2 g^{-1}). The higher EAS in 2% Pt/N-Me-C is attributable to the ultra low Pt loading featuring with small particle sizes and isolated distributions.

RDE and RRDE measurements

ORR activity and four-electron selectivity (H_2O_2 yield) data for 2% Pt/N-Me-C catalyst, including five controls (C, N-C, N-Me-C, 2% Pt/C, and 2% Pt/N-Me-C catalyst after 5000 cycles from 0 to 1.0 V in N_2-saturated 0.5 M H_2SO_4 solution) are shown in Fig. 8. While pyrolysis is beneficial for an improvement in the ORR activity of carbon black (Ketjen Black EC 300J), the pyrolyzed carbon sample still exhibited poor ORR performance and suffered from high peroxide yields. This suggests that the carbon surface provides few active sites for oxygen reduction, mainly to H_2O_2 through a two-electron route. Similar results also were reported for other carbon materials, such as Vulcan XC-72 and Black Pearl 2000.[56] In the case of the pyrolyzed N-C sample, the introduction of nitrogen leads to an obvious improvement in activity, evidenced by the positive shifts of the onset ORR potential from 0.52 to 0.79 V and of the half-wave potential from 0.28 to 0.45 V, when compared with the nitrogen-free pyrolyzed carbon black sample. At the same time, the H_2O_2 yields decrease to 17% at 0.40 V. It has been indicated that, theoretically and experimentally,[12,40,41] nitrogen can be viewed as an n-type dopant into a carbon graphene sheet forming disordered nanostructures (pyridinic and quaternary N) and donating more electrons, as the two possible ways to facilitate oxygen reduction at carbonaceous materials. However, such active sites appear unable to effectively electrocatalytically reduce oxygen to water through a four-electron route.

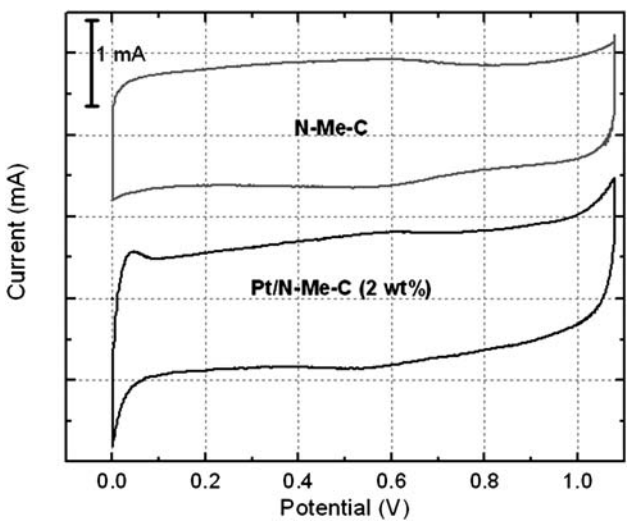

Fig. 7 CV for N-Me-C and 2% Pt/N-Me-C recorded in 0.5 M H_2SO_4 at room temperature, scan rate: 10 mV s^{-1}.

The simultaneous additions of nitrogen and transition metals in the N-Me-C sample dramatically improved the ORR activity and selectivity *via* four-electron reduction to H_2O. Typically, measured ORR onset and half-wave potentials are as high as 0.82 and 0.71 V. At the same time, the determined H_2O_2 yield has been reduced to 7% at 0.40 V. Noteworthy, a well-defined current plateau controlled by mass transfer, following charge-transfer kinetics control potential range, was observed for the N-Me-C sample, attesting to the high density and uniform distribution of ORR active sites on the catalyst.[57] As mentioned earlier, the role of transition metals in active ORR sites has been the subject of an ongoing controversy for quite some time. However, recently considerable effort in characterizing such kinds of non-precious metal catalyst suggested that the formed ORR active sites are greatly dependent on the nitrogen precursors and employed transition metals.[8,30] Compared with an ethylene diamine-derived catalyst, the polyaniline-derived one exhibited much higher activity and stability, indicating differences in the nature of the active site in both cases, with possible involvement of the metal in the ORR process in the latter.[8,30] At the same time, the active sites related to Co and Fe species are unlike in nature. Co species might majorly promote nitrogen doping into carbon graphene forming abundant pyridinic structures as potential active sites. Based on Mossbauer adsorption spectroscopy[58] and X-ray absorption,[30,59] another contrasting mechanism indicated that, even at the high pyrolysis temperature, Fe can be stabilized by a nitrogen-carbon network in the form of pyrrolic and/or pyridinic species, and seems to participate directly in the active ORR sites. These active sites possess much higher ORR activity and better selectivity than the sites formed with assistance of Co species.[8,30]

In the case of the 2% Pt/N-Me-C catalyst, the deposition of Pt (0.006 mg_{-Pt} cm^{-2} on RDE) leads to a significant enhancement in ORR activity, showing 140 and 80 mV positive shifts in the onset and half-wave potentials, respectively, when compared with its supporting materials (N-Me-C). In further comparison to 2% Pt catalyst supported on conventional carbon black with the same Pt loading (0.006 mg_{-Pt} cm^{-2} on RDE), while their onset potentials are nearly identical around 0.95 V, 2% Pt/N-Me-C exhibited a positive shift of 90 mV in half-wave potential, indicating a much higher density of ORR active sites derived from N-Me-C

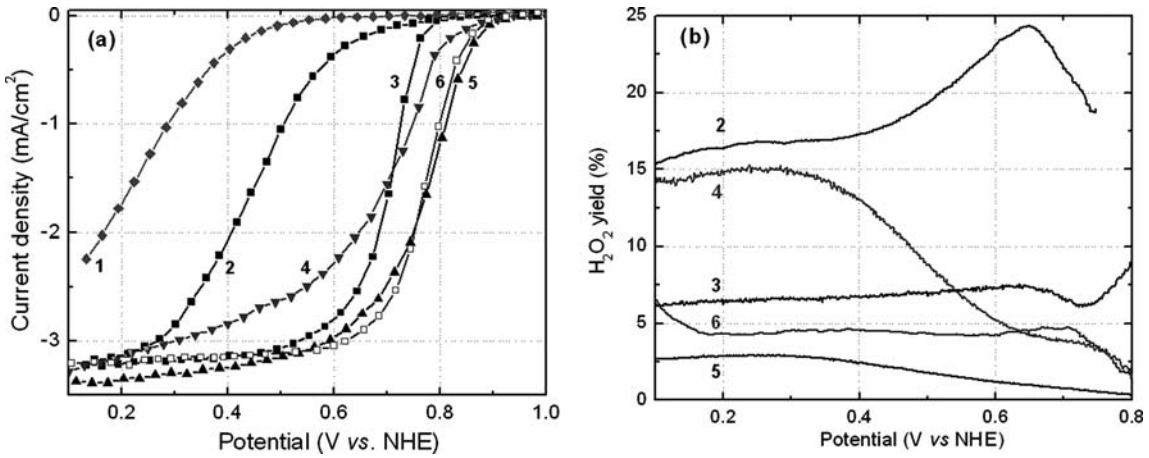

Fig. 8 Steady-state RDE polarization plots (a) and RRDE H_2O_2 yield (b) recorded with various samples: (1) pyrolyzed carbon black; (2) N-C; (3) N-Me-C; (4) 2% Pt/C; (5) 2% Pt/N-Me-C; (6) 2% Pt/N-Me-C after 5000 cycles. Electrolyte: 0.5 M H_2SO_4 at 25 °C; rotating rate: 900 rpm; catalyst loading: 0.3 mg cm^{-2} for non-Pt sample and 0.006 mg$_{\text{-Pt}}$ cm^{-2} for 2% Pt/C and 2% Pt/N-Me-C catalysts.

supporting materials. The long-term catalytic activity of 2% Pt/N-Me-C catalyst was evaluated during the CV "aging" study from 0 to 1.0 V in N_2-saturated 0.5 M H_2SO_4 solution. Consistent with the HR-TEM analysis, after 5000 cycles, 2% Pt/N-Me-C catalyst shows little ORR performance loss at kinetic potential range, except for a slight increase in H_2O_2 yield, probably due to the formation of oxygen-containing functional groups on the catalyst during cycling. As for commercial E-TEK 20% Pt/C catalyst, 5000 CV cycles typically caused a performance loss of 70% when compared with its initial ORR activity. Recently, by using functionalized graphene sheets (FGS) as supporting materials, a much more stable 20 wt% Pt/FGS catalyst has been developed by Lin and co-workers, but it still suffers a 50% ORR activity loss after 5000 RDE cycling degradation.[26] So the observation of RDE cycling stability for the 2% Pt/N-Me-C catalyst reinforces the conclusion that a combination of ultra-low Pt loading morphology with N-Me-C supports could provide a beneficial stabilization effect for loaded Pt particles.

Fuel cell performance

In order to examine fuel cell performance and Pt utilization, 2% N-Me-C and 2% Pt/C catalysts were tested as cathodes using the membrane electrode assembly (MEA) technique. As the total cathode loading including supporting materials is controlled at 2 mg cm^{-2}, Pt loading in these 2% Pt cathodes is around 0.04 mg$_{\text{-Pt}}$ cm^{-2}. Meanwhile, a standard Pt cathode with a Pt loading of 0.2 mg$_{\text{-Pt}}$ cm^{-2} using E-TEK 20% Pt/C catalyst was used as a reference in fuel cell tests. Fig. 9a shows their fuel cell polarization plots and power density data recorded in a H_2-air cell at a temperature of 80 °C and back pressures of 30/30 psig. Ohmic potential drop was not compensated for in these data. It is quite significant that an ultra-low Pt loading of 0.04 mg-$_{\text{Pt}}$cm^{-2} in the 2% Pt/N-Me-C cathode is effective in generating a current density of *ca.* 0.14 and 0.59 A cm^{-2} at cell voltages of 0.80 and 0.65 V, respectively. Also, the power density at 0.65 V is around 0.38 W cm^{-2}. The corresponding performance is much higher than that of 2% Pt/C that generated 0.10 A cm^{-2} at 0.80 V and 0.42 A cm^{-2} at 0.65 V. A similar attempt at lowering Pt loading to 0.04 mg cm^{-2} also had been reported by Mukerjee and his co-workers,[60] whose ultra-low Pt cathode was prepared by the dual ion-beam assisted deposition (dual IBAD) method on the surface of a non-catalyzed gas diffusion layer (GDL) substrate. Under approximately similar fuel cell testing conditions (H_2/air operation at 80 °C, Nafion® 212 membrane) but higher back pressure (50/60 psig), current densities obtained at cell voltages of 0.80

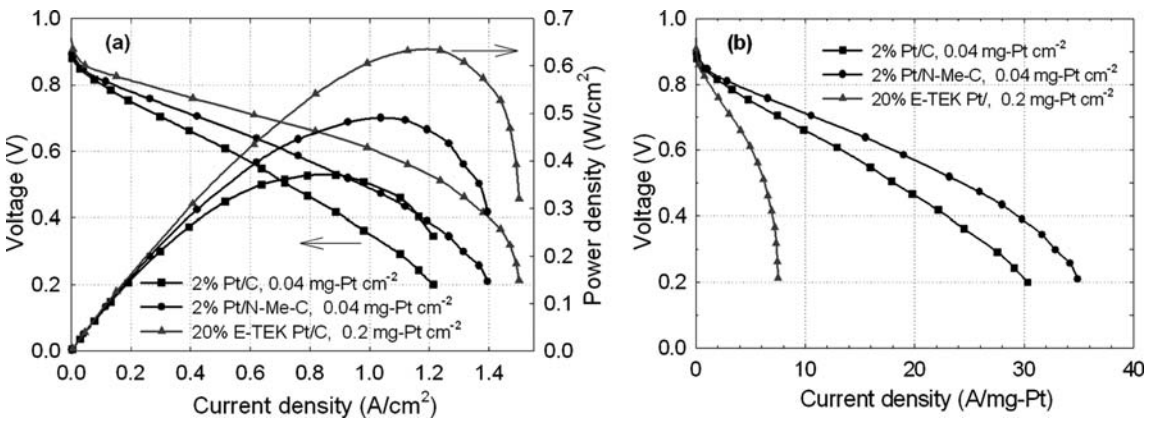

Fig. 9 Fuel cell testing for 2% Pt (0.04 mg$_{\text{-Pt}}$ cm^{-2}) and E-TEK 20% Pt/C (0.2 mg$_{\text{-Pt}}$ cm^{-2}) cathode catalysts using H_2-air: cell temperature: 80 °C; back pressures: 30/30 psig; membrane: Nafion® 212, (a) apparent polarization curves; (b) polarization curves *versus* mass of Pt.

and 0.65 V were around 0.10 and 0.40 A cm^{-2}, respectively. As a result, the area specific power density was 0.27 W cm^{-2} at 0.65 V. The higher performance observed with the 2% Pt/N-Me-C catalyst implies that, apart from the possible difference in Pt utilization between our 2% Pt/N-Me-C catalyst and the Pt electrode from dual IBAD, it appears that N-Me-C significantly enhance fuel cell performance, approximately generating an extra 30% (0.19 A cm^{-2} and of 0.11 W cm^{-2}) current density and a power density at 0.65 V. When directly comparing their fuel cell polarization plots with E-TEK 20% Pt/C cathode with five time higher Pt loading (0.2 mg-Pt cm^{-2}), the performance of 2% Pt/N-Me-C (0.04 mg-Pt cm^{-2}) is only lower by factors of 1.3 and 1.6 at 0.80 and 0.65 V, respectively. Typical thickness for the 2% Pt/N-Me-C catalyst is around 30 μm when total catalyst loading (mostly carbon materials) is 2.0 mg cm^{-2}, which is much thicker in comparison to the E-TEK 20% Pt/C cathode with a thickness of 10 μm (total 1.0 mg cm^{-2} including carbon support). Thus, it seems that performance of the 2% Pt/N-Me-C cathode retains a significant limitation by oxygen and proton transfers. To further compare the Pt utilization in these cathodes, the performance was re-plotted *versus* unit of Pt mass, as shown in Fig. 9b. It can be seen that mass activity (A $mg_{\text{-Pt}}^{-1}$) of 2% Pt/N-Me-C increased by factors of 1.4 and 3.5 at a voltage of 0.65 V, when compared with 2% Pt/C and E-TEK 20% Pt/C cathodes, respectively. So the significant improvement in mass activity in the 2% Pt/N-Me-C catalyst is mainly attributable to the contribution of non-precious ORR active sites provided by the novel support (M-Me-C), and also partially to the smaller particle size due to its ultra-low Pt loading.

Conclusion

A new non-precious composite carbon material N-Me-C, featuring a magnetic property, doping of nitrogen atoms, and highly graphitic onion-like nanostructures, was synthesized by pyrolyzing a carbon black supported hexamethylene diamine-Me (Me: Co and Fe) complex, capable of high activity and four-electron selectivity for ORR. In order to achieve a reasonable balance between feasible costs and commercially viable application for fuel cell technology, Pt nanoparticles were anchored on the active N-Me-C supports with a Pt loading around 2.0 wt%. The configuration with ultra-low Pt loading is advantageous for improvements of Pt utilization and mitigation of Pt particle agglomeration due to smaller particle sizes and more isolated particle distributions. Based on electrochemical RDE cycling degradation test and morphology analysis, an enhanced stability of Pt catalyst was achieved. The N-Me-C carbon supporting materials proved not only to offer a remarkable support effect by geometrically and electronically modifying the loaded Pt particles, but also to provide a large amount of performing non-precious ORR active sites. So the hybrid cathode catalyst consisting of Pt and non-precious metal catalysts (with a Pt loading of 0.04 $mg_{\text{-Pt}}$ cm^{-2}) exhibited significantly improved overall performance in ORR, leading to an increase in mass activity (A $mg_{\text{-Pt}}^{-1}$), and a reduction in total costs of fuel cells (gauged in US$ kW^{-1}). Optimization of catalyst synthesis including non-precious active supporting materials and morphology of Pt nanoparticles could continuously improve activity and durability for such-fabricated hybrid cathodes. It would open a new way to make the non-precious catalyst, at least, partially replace the expensive Pt in PEFC application in the foreseeable future.

Acknowledgements

The authors acknowledge the financial support of this work from the Postdoctoral Science Foundation (2004035300), and National Natural Science Foundation of China (NSFC) (20435010, 20503012). We also appreciate Dr Huang Jiugui in Baoshan Iron & Steel Co. for his help to do HRTEM and other analysis.

References

1 J. X. Wang, F. A. Uribe, T. E. Springer, J. L. Zhang and R. R. Adzic, *Faraday Discuss.*, 2009, **140**, 347.
2 S. Walch, A. Dhanda, M. Aryanpour and H. Pitsch, *J. Phys. Chem. C*, 2008, **112**, 8464.
3 H. A. Gasteiger and N. M. Markovic, *Science*, 2009, **324**, 48.
4 H. Yano, M. Kataoka, H. Yamashita, H. Uchida and M. Watanabe, *Langmuir*, 2007, **23**, 6438.
5 K. Gong, F. Du, Z. Xia, M. Durstock and L. Dai, *Science*, 2009, **323**, 760.
6 R. Bashyam and P. Zelenay, *Nature*, 2009, **443**, 63.
7 C. W. B. Bezerra, L. Zhang, K. C. Lee, H. S. Liu, A. L. B. Marques, E. P. Marques, H. J. Wang and J. J. Zhang, *Electrochim. Acta*, 2008, **53**, 4937.
8 G. Wu, Z. W. Chen, K. Artyushkova, F. H. Garzon and P. Zelenay, *ECS Trans.*, 2008, **16**, 159.
9 G. Wu, G. Cui, D. Li, P.-K. Shen and N. Li, *J. Mater. Chem.*, 2009, **19**, 6581.
10 H. A. Gasteiger, S. S. Kocha, B. Sompalli and F. T. Wagner, *Appl. Catal., B*, 2005, **56**, 9.
11 M. Lefevre, E. Proietti, F. Jaouen and J. P. Dodelet, *Science*, 2009, **324**, 71.
12 T. Ikeda, M. Boero, S. F. Huang, K. Terakura, M. Oshima and J. Ozaki, *J. Phys. Chem. C*, 2008, **112**, 14706.
13 P. H. Matter, E. Wang and U. S. Ozkan, *J. Catal.*, 2006, **243**, 395.
14 G. Lalande, R. Cote, D. Guay, J. P. Dodelet, L. T. Weng and P. Bertrand, *Electrochim. Acta*, 1997, **42**, 1379.
15 H. Yoon, S. Ko and J. Jang, *Chem. Commun.*, 2007, 1468.
16 F. Su, Z. Tian, C. K. Poh, Z. Wang, S. H. Lim, Z. Liu and J. Lin, *Chem. Mater.*, 2010, **22**, 832.
17 G. Vijayaraghavan and K. J. Stevenson, *Langmuir*, 2007, **23**, 5279.
18 G. Wu, R. Swaidan, D. Y. Li and N. Li, *Electrochim. Acta*, 2008, **53**, 7622.
19 G. Wu, D. Y. Li, C. S. Dai, D. L. Wang and N. Li, *Langmuir*, 2008, **24**, 3566.
20 B. Fang, J. H. Kim, M. Kim, M. Kim and J.-S. Yu, *Phys. Chem. Chem. Phys.*, 2009, **11**, 1380.
21 G. Wu, L. Li, J. H. Li and B. Q. Xu, *J. Power Sources*, 2006, **155**, 118.
22 G. Wu, L. Li, J. H. Li and B. Q. Xu, *Carbon*, 2005, **43**, 2579.
23 Y. Y. Shao, J. Liu, Y. Wang and Y. H. Lin, *J. Mater. Chem.*, 2009, **19**, 46.
24 G. Wu and B. Q. Xu, *J. Power Sources*, 2007, **174**, 148.
25 G. Wu, Y. S. Chen and B. Q. Xu, *Electrochem. Commun.*, 2005, **7**, 1237.
26 R. Kou, Y. Shao, D. Wang, M. H. Engelhard, J. H. Kwak, J. Wang, V. V. Viswanathan, C. Wang, Y. Lin, Y. Wang, I. A. Aksay and J. Liu, *Electrochem. Commun.*, 2009, **11**, 954.
27 Y. Zhao, R. Pasquarelli, T. Holme, J. Berry, D. Ginley and R. O'Hayre, *J. Mater. Chem.*, 2009, **19**, 7830.
28 J. D S. Maldonado, S. Morin and K. J. Stevenson, *Carbon*, 2006, **44**, 1429.
29 J. Lahaye, G. Nanse, A. Bagreev and V. Strelko, *Carbon*, 1999, **37**, 585.
30 G. Wu, K. Artyushkova, M. Ferrandon, J. Kropf, D. Myers and P. Zelenay, *ECS Trans*, 2009, **25**, 1299.
31 H. C. Sirk, S. A. Campbell and V. I. Birss, *Electrochem. Solid-State Lett.*, 2005, **8**, A104.

32 W. T. Lian, H. H. Song, X. H. Chen, L. X. Li, J. P. Huo, M. Zhao and G. Q. Wang, *Carbon*, 2008, **46**, 525.
33 B. S. Xu, X. W. Yang, X. M. Wang, J. J. Guo and X. G. Liu, *J. Power Sources*, 2006, **162**, 160.
34 V. Cherstiouk, P. A. Simonov and E. R. Savinova, *Electrochim. Acta*, 2003, **48**, 3851.
35 X. W. Yu and S. Y. Ye, *J. Power Sources*, 2007, **172**, 145.
36 F. A. de Bruijn, V. A. T. Dam and G. J. M. Janssen, *Fuel Cells*, 2008, **8**, 3.
37 G. Rimbu, C. Jackson and K. Scott, *J. Optoelectro. Adv. Mater.*, 2006, **8**, 611.
38 T. E. Wood, Z. Tan, A. K. Schmoeckel, D. O'Neill and R. Atanasoski, *J. Power Sources*, 2008, **178**, 510.
39 S. L. Gojkovic, S. Gupta and R. F. Savinell, *Electrochim. Acta*, 1999, **45**, 889.
40 S. Maldonado and K. J. Stevenson, *J. Phys. Chem. B*, 2005, **109**, 4707.
41 P. H. Matter, L. Zhang and U. S. Ozkan, *J. Catal.*, 2006, **239**, 83.
42 J. R. Pels, F. Kapteijn, J. A. Moulijn, Q. Zhu and K. M. Thomas, *Carbon*, 1995, **33**, 1641.
43 S. B. Yang, H. Q. Hu and G. H. Chen, *Carbon*, 2002, **40**, 277.
44 G. M. Fuge, C. J. Rennick, S. R. J. Pearce, P. W. May and M. N. R. Ashfold, *Diamond Relat. Mater.*, 2003, **12**, 1049.
45 J. W. Jang, C. E. Lee, S. C. Lyu, T. J. Lee and C. J. Lee, *Appl. Phys. Lett.*, 2004, **84**, 2877.
46 J. Haglund, A. F. Guillermet, G. Grimvall and M. Korling, *Phys. Rev. B: Condens. Matter*, 1993, **48**, 11685.
47 G. Wu, R. Swaidan and G. F. Cui, *J. Power Sources*, 2007, **172**, 180.
48 G. Wu, L. Li and B. Q. Xu, *Electrochim. Acta*, 2004, **50**, 1.
49 J. Zheng, T. C. Ekstrom, S. K. Gordeev and M. Jacob, *J. Mater. Chem.*, 2000, **10**, 1039.
50 V. Gubarevich, J. Kitamura, S. Usuba, H. Yokoi, Y. Kakudate and O. Odawara, *Carbon*, 2003, **41**, 2601.
51 Y. V. Butenko, S. Krishnamurthy, A. K. Chakraborty, V. L. Klznetsov, V. R. Dhanak, M. R. C. Hunt and L. Siller, *Phys. Rev. B*, 2005, **71**, 10.
52 P. Simon and Y. Gogotsi, *Nat. Mater.*, 2008, **7**, 845.
53 B. S. Xu, *New Carbon Mater.*, 2008, **23**, 289.
54 B. Y. Xia, J. N. Wang, X. X. Wang, J. J. Niu, Z. M. Sheng, M. R. Hu and Q. C. Yu, *Adv. Funct. Mater.*, 2008, **18**, 1790.
55 G. Faubert, D. Guay and J. P. Dodelet, *J. Electrochem. Soc.*, 1998, **145**, 2985.
56 H. Wang, R. Cote, G. Faubert, D. Guay and J. P. Dodelet, *J. Phys. Chem. B*, 1999, **103**, 2042.
57 J. Maruyama and I. Abe, *J. Electroanal. Chem.*, 2003, **545**, 109.
58 L. Bouwkamp-Wijnoltz, W. Visscher, J. A. R. van Veen, E. Boellaard, A. M. van der Kraan and S. C. Tang, *J. Phys. Chem. B*, 2002, **106**, 12993.
59 T. Bae, D. A. Tryk and D. A. Scherson, *J. Phys. Chem. B*, 1998, **102**, 4114.
60 M. S. Saha, A. F. Gullá, R. J. Allen and S. Mukerjee, *Electrochim. Acta*, 2006, **51**, 4680.

